



# Cu-SAPO-56, a potential catalyst for the selective catalytic reduction of NO<sub>x</sub> by NH<sub>3</sub>

Lei Xu<sup>a</sup>, Ye Wang<sup>b,c</sup>, Yi Cao<sup>d,e</sup>, Feng Zhang<sup>a</sup>, Yu Song<sup>a</sup>, Chunling Yu<sup>a</sup>, Peng Tian<sup>b</sup>, Lijing Sun<sup>a,\*</sup>

<sup>a</sup> School of Light Industry and Chemical Engineering, Dalian Polytechnic University, #1 Qinggongyuan, Dalian, 116034, China

<sup>b</sup> National Engineering Laboratory for Methanol to Olefins, Dalian Institute of Chemical Physics, Chinese Academy of Sciences, Dalian, 116023, Liaoning, China

<sup>c</sup> Dalian National Laboratory for Clean Energy, Dalian Institute of Chemical Physics, Chinese Academy of Sciences, Dalian, 116023, Liaoning, China

<sup>d</sup> School of Material Science and Chemical Engineering, Ningbo University, Ningbo, 315211, China

<sup>e</sup> National Engineering Laboratory for Methanol to Olefins, Dalian National Laboratory for Clean Energy, Dalian Institute of Chemical Physics, Chinese Academy of Sciences, Dalian, 116023, China

## ARTICLE INFO

### Keywords:

Cu-SAPO-56  
NH<sub>3</sub>-SCR  
Hydrothermal stability  
Cu species  
Acidity

## ABSTRACT

A novel Cu-exchanged catalyst, Cu-SAPO-56 prepared by direct ion exchange method, was studied for NH<sub>3</sub>-SCR reaction. Cu-SAPO-56 exhibits excellent NH<sub>3</sub>-SCR activity and hydrothermal stability. The NO<sub>x</sub> conversion of Cu-SAPO-56 maintains more than 90 % at a wide temperature range between 250 °C and 400 °C even after a rigorous steam treatment (800 °C for 16 h or 50 °C for 24 h). The isolated Cu<sup>2+</sup> ions located in double 6-ring of AFX structure are determined as the catalytic active sites. Both of Cu content and Si content in Cu-SAPO-56 play critical roles in NH<sub>3</sub>-SCR activity and hydrothermal stability. The excellent catalytic performance and strong hydrothermal stability exhibits the huge application potential of Cu-SAPO-56 for NH<sub>3</sub>-SCR reaction.

## 1. Introduction

Selective catalytic reduction of NO<sub>x</sub> (nitrogen oxides, including NO, NO<sub>2</sub> and N<sub>2</sub>O) by ammonia (NH<sub>3</sub>-SCR) is one of the most effective technologies to reduce NO<sub>x</sub> emission [1]. The more and more stringent NO<sub>x</sub> emission standards prompt the development of high efficient catalysts for the NH<sub>3</sub>-SCR reaction. Cu-exchanged zeolite with excellent catalytic activity and environmentally benign seems to be a promising candidate [2,3]. Mesoporous zeolite Cu-ZSM-5 was proposed as an efficient catalyst for NH<sub>3</sub>-SCR by Iwamoto in 1986 [4]. Unfortunately, the macroporous and mesoporous zeolites, such as Cu-Beta, Cu-FAU and Cu-MFI, suffer from dealumination processes which lead to a bad hydrothermal stability [5,6].

Recently, the micropore Cu-exchanged zeolites such as Cu-SSZ-13 and Cu-SAPO-34 with better NH<sub>3</sub>-SCR activity and hydrothermal stability have been proposed as NH<sub>3</sub>-SCR catalysts [7]. The better NH<sub>3</sub>-SCR performance of Cu-CHA is attributed to the preferential coordination of Cu<sup>2+</sup> ions at double 6-ring (D6R) cages which are proved to be the NH<sub>3</sub>-SCR activity sites. And the less dealumination confined by the small 8-ring channels contributes to its strong resistance for steam treatment [8,9]. In addition to CHA, other Cu-exchanged micropore zeolites, such

as Cu-SSZ-16, Cu-SSZ-39 and Cu-LTA, containing D6R cages in the structures also have been found as suitable catalysts for NH<sub>3</sub>-SCR [10–12].

The framework of Cu-SSZ-16 is AFX structure formed by three types of cages: D6R cage, GME cage and large AFT cage with a smaller pore size (3.4 × 3.6 Å) than CHA pore size (3.8 × 3.8 Å). Lobo et al. found Cu-SSZ-16 had a comparable NH<sub>3</sub>-SCR activity to Cu-SSZ-13 indicating its potential in NH<sub>3</sub>-SCR catalysts [13]. However, Cu-SSZ-16 is restricted by the poor hydrothermal stability. The NO<sub>x</sub> conversion of Cu-SSZ-16 decreases obviously even after a mild hydrothermal treatment (750 °C for 7 h). The poor hydrothermal stability probably caused by the obvious crystallinity decrease and loss of active Cu<sup>2+</sup> ion sites in aluminosilicate framework under H<sub>2</sub>O attack [14,15]. Compared to aluminosilicate zeolites, silicoaluminophosphate (SAPO) molecular sieves exhibit better hydrothermal stability [16–19]. The desilication defects can be healed by the migration of the extra-framework P atoms during the hydrothermal treatment. At the same time, the surface CuO particulates in SAPO molecular sieves may transform to active isolated Cu<sup>2+</sup> ions which further improves the NO<sub>x</sub> conversion [20,21]. Thus, SAPO molecular sieves Cu-SAPO-56 with same AFX structure is a potential catalyst with good NH<sub>3</sub>-SCR activity and better hydrothermal stability. However, the

\* Corresponding author.

E-mail address: [sunlj@dlpu.edu.cn](mailto:sunlj@dlpu.edu.cn) (L. Sun).

<https://doi.org/10.1016/j.micromeso.2023.112978>

Received 11 September 2023; Received in revised form 21 December 2023; Accepted 30 December 2023

Available online 31 December 2023

1387-1811/© 2023 Published by Elsevier Inc.

related research about its  $\text{NH}_3$ -SCR activity and hydrothermal stability is rare.

Cu exchanged SAPO molecular sieves generally prepared by a time-consuming post-treatment method contained calculation for removing templates,  $\text{NH}_4^+$  ion exchange and  $\text{Cu}^{2+}$  ion exchange in aqueous solution. This process may cause the structural damage and crystallinity loss due to the high sensitivity of the SAPO frameworks to  $\text{H}_2\text{O}$  at low temperature [22]. By contrast, direct ion exchange method only contains  $\text{Cu}^{2+}$  ion exchange procedure which employs the amine templates for Cu-exchange. As the pores and cages are occupied by organic amines and the negative Si–O–Al bonds are balanced by protonated amines, SAPO framework is more resistant during the direct ion exchange process [23].

Herein, we employed direct ion exchange method to prepare Cu-SAPO-56 with different Si and Cu contents. We also reported the catalytic properties of Cu-SAPO-56 for  $\text{NH}_3$ -SCR. Nuclear magnetic resonance (NMR), electron paramagnetic resonance (EPR),  $\text{NH}_3$  temperature-programmed desorption ( $\text{NH}_3$ -TPD),  $\text{H}_2$  temperature-programmed reduction ( $\text{H}_2$ -TPR),  $\text{N}_2$  adsorption–desorption, X-ray diffraction (XRD), X-ray fluorescence (XRF) and scanning electron microscopy (SEM) measurements were performed to investigate the physicochemical characteristics and the active species of Cu-SAPO-56. More importantly, the influences of Si and Cu contents to the  $\text{NH}_3$ -SCR activity and hydrothermal stability were further revealed over Cu-SAPO-56 in our work.

## 2. Materials and methods

### 2.1. Raw materials

The raw materials used include phosphoric acid ( $\text{H}_3\text{PO}_4$ , 85 wt%), tetraethyl orthosilicate (TEOS, 99 wt%), pseudoboehmite ( $\text{Al}_2\text{O}_3$ , 77 wt%), copper (II) acetate pentahydrate ( $\text{Cu}(\text{Ac})_2 \cdot 5\text{H}_2\text{O}$ , 98 wt%), ammonium nitrate ( $\text{NH}_4\text{NO}_3$ , 99 wt%), N,N,N',N'-tetramethyl-1,6-hexanediamine (TMHD, 99 wt%) and triethylamine (TEA, 99 wt%). All the chemicals were obtained from commercial suppliers and used directly without further purification.

### 2.2. Synthesis of SAPO-56

SAPO-56 was synthesized by using TMHD as a template. Typically, pseudoboehmite was first dissolved into a certain amount of distilled water followed by the addition of phosphoric acid, TEOS and TMHD. The molar compositions of the final gels were 1.0  $\text{Al}_2\text{O}_3$ /1.2  $\text{P}_2\text{O}_5$ /2.5 TMHD/(0.4–0.9)  $\text{SiO}_2$ /58 $\text{H}_2\text{O}$ . The crystallization was carried out in Teflon-lined autoclaves at 210 °C for 24 h under rotation. The products were collected by centrifugation, washed with deionized  $\text{H}_2\text{O}$ , and dried at 100 °C for 24 h.

### 2.3. Catalyst preparation

The Cu-SAPO-56 catalysts were prepared by conventional ion exchange method and direct ion exchange method. For the conventional ion exchange method, the as-synthesized molecular sieves were calcined at 600 °C for 3 h to remove the templates. The calcined molecular sieves were put into the  $\text{NH}_4\text{NO}_3$  solution (3.66 mol/L) and stirred at 80 °C for 2 h. And the molecular sieves were collected by centrifugation, washed with deionized  $\text{H}_2\text{O}$ , and dried at 100 °C for 24 h. Then, the molecular sieves were put into the copper (II) acetate solution and stirred at 50 °C for 4 h. Afterwards, the catalysts were collected by centrifugation, washed with deionized  $\text{H}_2\text{O}$ , and dried at 100 °C for 24 h and calcined at 600 °C for 3 h to remove the organics.

For the direct ion exchange method, the as-synthesized molecular sieves were directly put into the copper (II) acetate solution and stirred at 50 °C for 4 h. Afterwards, the catalysts were collected by centrifugation, washed with deionized  $\text{H}_2\text{O}$ , and dried at 100 °C for 24 h. Then,

the Cu-exchanged samples were calcined at 600 °C for 3 h to remove the organics.

### 2.4. Characterizations

The powder XRD patterns were recorded on a PANalytical X'Pert PRO X-ray diffractometer with Cu-K $\alpha$  radiation ( $\lambda = 1.54059 \text{ \AA}$ ) at 40 kV and 40 mA. Element analyses of the samples were tested on a Philips Magix-601 X-ray fluorescence (XRF) spectrometer. The crystal morphology of the samples was observed by a Hitachi S-3400 N scanning electron microscopy (SEM). Textural properties of the calcined samples were determined by  $\text{N}_2$  adsorption at 77 K on a Micromeritics ASAP 2020 system. The total surface area was calculated based on the Brunauer-Emmett-Teller (BET) equation, and the micropore volume and surface area were determined by using the t-plot method. The  $^{29}\text{Si}$  MAS NMR spectra was recorded on a Bruker Avance III 600 spectrometer equipped with a 14.1-T wide-bore magnet. The resonance frequencies was 119.2 MHz. The spinning rates of the samples at the magic angle for was 6 kHz. The reference material for the chemical shift (in parts per million (ppm)) determination was the sodium salt of 2,2-dimethyl-2-silapentane-5-sulfonate (DSS). The temperature-programmed desorption of ammonia ( $\text{NH}_3$ -TPD) experiments were conducted in a Micromeritics Autochem II 2920 device. 100 mg calcined sample particles (40–60 mesh) were loaded into a U-quartz tube and pretreated at 650 °C for 1 h in He flow (30 mL/min) to remove the impurities, and then treated in a gas mixture of 2 %  $\text{NH}_3$ -98 % He flow (30 mL/min) at 120 °C to saturate the sample surface with  $\text{NH}_3$  adsorption (60 min). After this, He flow (30 mL/min) purged through the sample for 30 min to remove the weakly adsorbed  $\text{NH}_3$  molecules. The measurement of the desorbed  $\text{NH}_3$  was performed from 100 to 600 °C (10 °C/min) under He flow (30 mL/min).

Electron paramagnetic resonance (EPR) was performed on a Bruker A 200. 20 mg calcined sample was pre-treated in pure  $\text{N}_2$  at 120 °C for 12 h, and finally sealed into a quartz tube for characterization. During spectral collection, microwave power was 2 mW, and frequency was 9.52 GHz. The sweep width was 2000 G and sweep time was 84 s, modulated at 100 kHz with a 2 G amplitude. A time constant of 41 ms was used. The spectrum was collected at  $-171 \text{ }^\circ\text{C}$ . Quantification of isolated  $\text{Cu}^{2+}$  was conducted by using copper sulfate solution as a standard (at  $-171 \text{ }^\circ\text{C}$ ).

The temperature-programmed reduction of hydrogen ( $\text{H}_2$ -TPR) was obtained on a Micromeritics Autochem II 2920 device. 100 mg calcined sample particles (40–60 mesh) were pretreated at 500 °C for 30 min in 2 %  $\text{O}_2$ /He flow (30 mL/min) to remove the impurities and then cooled down to 100 °C by purging in Ar (30 mL/min). The  $\text{H}_2$ -TPR was treated from 100 to 900 °C with a rate of 10 °C/min under a 10 %  $\text{H}_2$ -90 % Ar flow (30 mL/min). A TCD detector was used to detect the consumption of  $\text{H}_2$ .

### 2.5. Catalyst evaluation

The  $\text{NH}_3$ -SCR reaction was tested by using 100 mg of catalyst (60–80 mesh) diluted by 400 mg of quartz beads (60–80 mesh) in a fixed bed quartz reactor. To determine the temperature of catalyst, the thermal couple was placed in the centre of catalyst bed. Before entering the reactor, the reactant gases were regulated by mass-flow controllers (Brookers). All gas lines were heated to 100 °C to prevent the condensation of vapor. The composition of the reactant gases was as follows: 500 ppm of  $\text{NO}$ , 500 ppm of  $\text{NH}_3$ , 6.1 % of  $\text{O}_2$ , 6.4 % of  $\text{H}_2\text{O}$  and balanced with  $\text{N}_2$  with the flow rate of 320 mL/min. The gas hourly space velocity (GHSV) was 180,000  $\text{h}^{-1}$ . The concentrations of  $\text{NO}_x$  ( $\text{NO}$ ,  $\text{NO}_2$  and  $\text{N}_2\text{O}$ ) in the inlet and outlet gases were continually analyzed by a Tensor 27, Bruker Fourier transform infrared (FTIR) spectrometer equipped with a 2 m gas cell. All catalysts were pretreated in the reactant gases at 550 °C for 2 h before activity test. Catalytic activity tests were carried out over the temperature range of 150–550 °C. And before

**Table 1**  
Direct ion-exchange conditions<sup>a</sup> and elemental compositions of the samples.

Sample	Cu(Ac) <sub>2</sub> concentration (0.01 mol/L)	Composition <sup>b</sup>	Cu content <sup>b</sup> (wt %)
S56-0.13Si	–	Al <sub>0.469</sub> P <sub>0.395</sub> Si <sub>0.136</sub> O <sub>2</sub>	0
S56-0.16Si	–	Al <sub>0.465</sub> P <sub>0.369</sub> Si <sub>0.166</sub> O <sub>2</sub>	0
S56-0.22Si	–	Al <sub>0.431</sub> P <sub>0.351</sub> Si <sub>0.218</sub> O <sub>2</sub>	0
S56-0.13Si-1.8Cu <sup>c</sup>	2.5	Al <sub>0.480</sub> P <sub>0.392</sub> Si <sub>0.128</sub> O <sub>2</sub>	1.75
S56-0.13Si-2.6Cu <sup>c</sup>	6.3	Al <sub>0.483</sub> P <sub>0.388</sub> Si <sub>0.129</sub> O <sub>2</sub>	2.64
S56-0.13Si-3.7Cu <sup>c</sup>	12	Al <sub>0.482</sub> P <sub>0.388</sub> Si <sub>0.130</sub> O <sub>2</sub>	3.67
S56-0.13Si-4.6Cu <sup>c</sup>	15	Al <sub>0.486</sub> P <sub>0.386</sub> Si <sub>0.128</sub> O <sub>2</sub>	4.64
S56-0.16Si-3.6Cu <sup>c</sup>	10	Al <sub>0.470</sub> P <sub>0.368</sub> Si <sub>0.162</sub> O <sub>2</sub>	3.64
S56-0.22Si-3.8Cu <sup>c</sup>	5.0	Al <sub>0.435</sub> P <sub>0.341</sub> Si <sub>0.224</sub> O <sub>2</sub>	3.76
Cu-SAPO-56-CIE <sup>d</sup>	3.0	Al <sub>0.467</sub> P <sub>0.372</sub> Si <sub>0.161</sub> O <sub>2</sub>	2.43

<sup>a</sup> The liquid (mL)/solid (g) ratio for Cu ion exchange is 10 (80 °C, 5 h). <sup>b</sup> Determined by XRF.

<sup>c</sup> The Cu-SAPO-56 was prepared by direct ion exchange method.

<sup>d</sup> The Cu-SAPO-56 was prepared by conventional ion exchange method.

recording the activity results, the reaction was holding at each temperature for 40min. The NO<sub>x</sub> conversion and N<sub>2</sub> selectivity were calculated by using the following formula (1) and (2), respectively:

$$\text{NO}_x \text{ conversion} = \frac{(\text{NO} + \text{NO}_2 + \text{N}_2\text{O})_{\text{in}} - (\text{NO} + \text{NO}_2 + \text{N}_2\text{O})_{\text{out}}}{(\text{NO} + \text{NO}_2 + \text{N}_2\text{O})_{\text{in}}} \times 100\% \quad (1)$$

$$\text{N}_2 \text{ selectivity} = \left[ 1 - \frac{2(\text{N}_2\text{O})_{\text{out}}}{(\text{NO} + \text{NO}_2 + \text{N}_2\text{O})_{\text{in}} - (\text{NO} + \text{NO}_2 + \text{N}_2\text{O})_{\text{out}}} \right] \times 100\% \quad (2)$$

## 2.6. Hydrothermal stability evaluation

After a standard NH<sub>3</sub>-SCR evaluation, the samples were further heated to 600 °C in dry air for ca. 15 min in the quartz reactor. And then, a gas flow containing 10 % water balanced with N<sub>2</sub> and air passed through the sample at 800 °C for 16 h to make a high-temperature hydrothermal treatment. For the low temperature steam treatment, a gas flow containing 10 % water balanced with N<sub>2</sub> and air passed through the sample at 50 °C for 24 h. And the total flow rate was 253 mL/min. Before any characterization or evaluation, the steaming treated samples were further heated to 600 °C in dry air and then kept in oven at 120 °C.

## 3. Results and discussion

### 3.1. Synthesis and characterizations of Cu-SAPO-56

As the Si content may influence the NH<sub>3</sub>-SCR activity and hydrothermal stability of Cu-exchanged molecular sieve catalysts, SAPO-56 with various Si contents have been firstly synthesized with TMHD as the template according to the previous report [24]. The product compositions of SAPO-56 are listed in Table 1. The Si content can be adjusted from 0.136 to 0.218 by altering the dosage of silica source. The SAPO-56 precursors are named as S56-xSi, while x represents the Si content. As seen in Fig. 1, XRD patterns for the as-synthesized SAPO-56 precursors are indexed to the typical AFX structure. No impurity phases or amorphous are observed indicating the purity of the as-synthesized SAPO-56. The SEM image of S56-0.13Si is shown in Fig. 2. The sample presents typical hexagonal platelet morphology of SAPO-56 with a particle size of ca. 6–12 μm.

The Cu-SAPO-34 was first prepared by conventional ion exchange method (named as Cu-SAPO-56-CIE). The XRD pattern of Cu-SAPO-56-CIE is shown in Fig. 1. The crystallinity of Cu-SAPO-56-CIE decreases dramatically and a lot of amorphous phase is formed after conventional ion exchange process. To improve the structure stability of Cu-SAPO-56, direct ion exchange method was employed to prepare Cu-SAPO-56 with

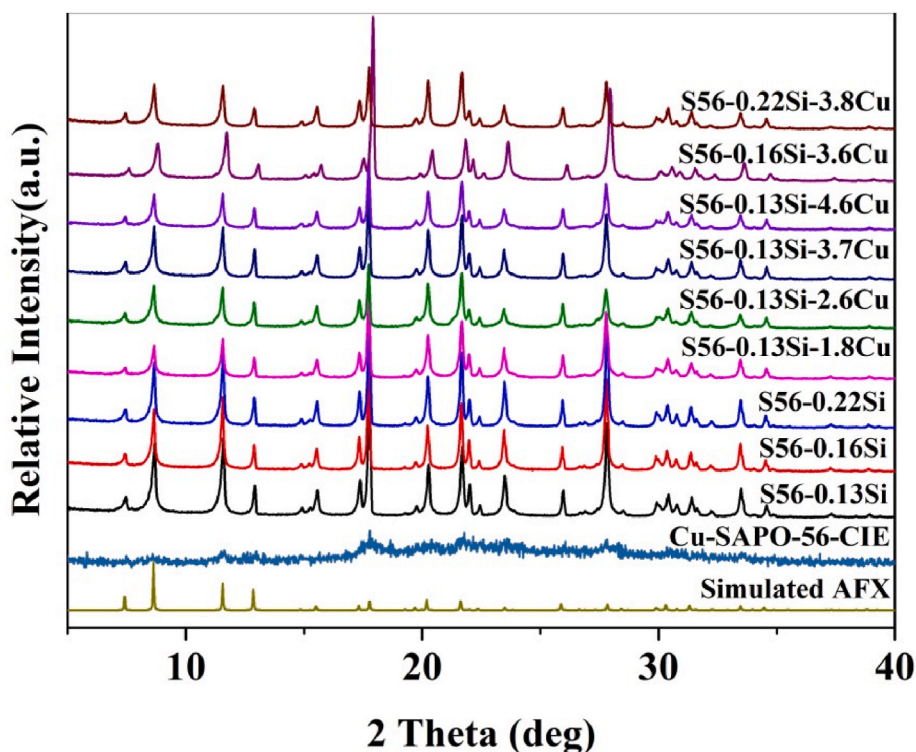


Fig. 1. XRD patterns of all the samples.

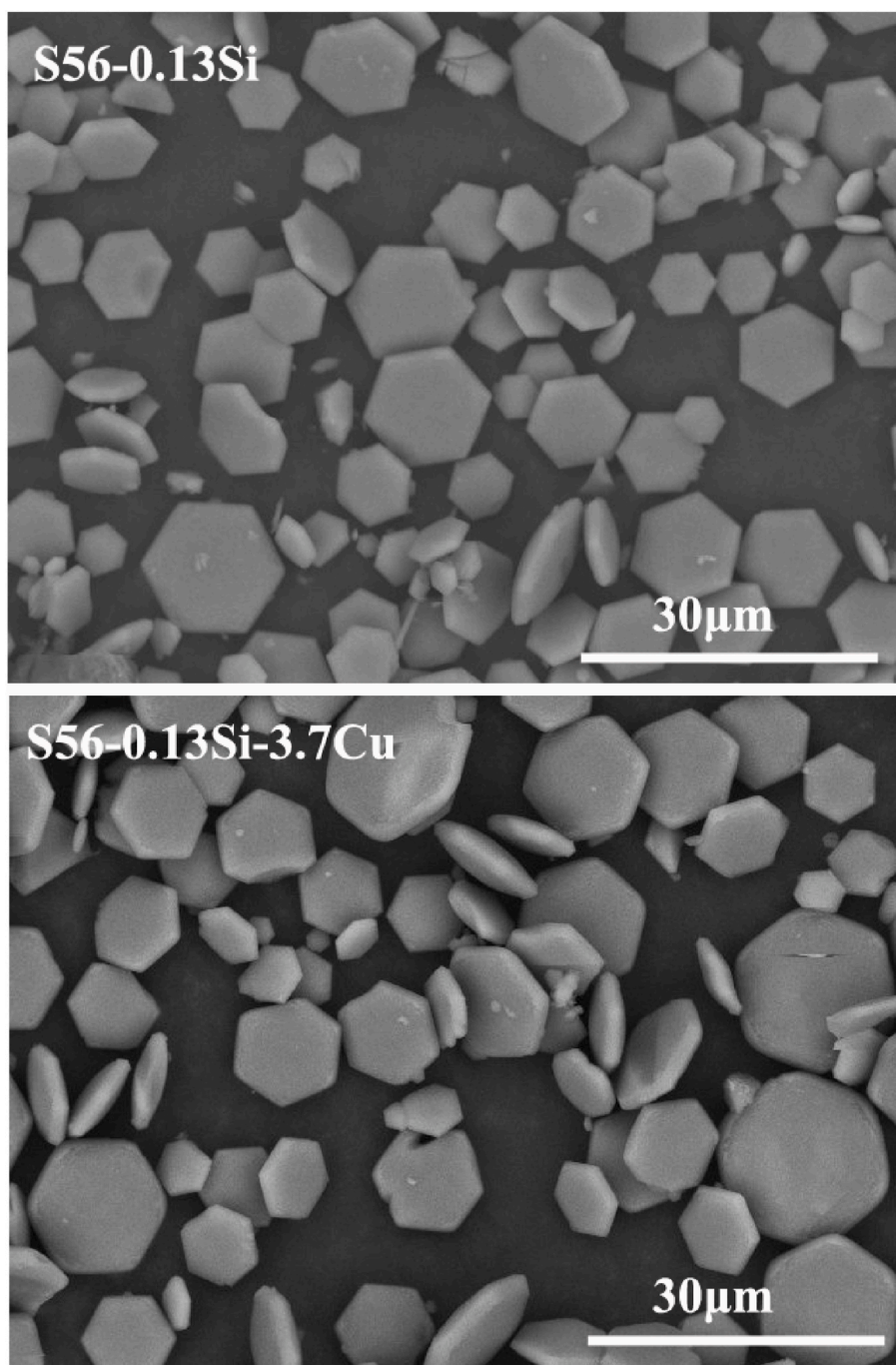


Fig. 2. SEM images of sample S56-0.13Si and S56-0.13Si-3.7Cu.

Table 2  
Textual properties of the samples.

Sample	Surface area ( $\text{m}^2 \text{g}^{-1}$ )			Pore volume ( $\text{cm}^3 \text{g}^{-1}$ )	
	$S_{\text{total}}^a$	$S_{\text{micro}}^b$	$S_{\text{ext}}^c$	$V_{\text{total}}$	$V_{\text{micro}}^d$
S56-0.13Si	617	534	83	0.31	0.26
S56-0.13Si-1.8Cu	570	486	84	0.30	0.23
S56-0.13Si-2.6Cu	548	463	85	0.29	0.22
S56-0.13Si-3.7Cu	537	454	84	0.29	0.22

<sup>a</sup> BET surface area.

<sup>b</sup> *t*-plot micropore surface area.

<sup>c</sup> *t*-plot external surface area.

<sup>d</sup> *t*-plot micropore volume.

varied Si and Cu contents [25]. The Cu-SAPO-56 samples are named as S56-xSi-yCu, while x and y represent the Si and Cu contents, respectively. The XRD patterns of the Cu-SAPO-56 samples are displayed in Fig. 1. All the XRD patterns remain the typical AFX structure without amorphous phase. There are no peaks at  $35.3^\circ$  and  $38.5^\circ$ , proving the absence of CuO species [21] and the advantage of the direct ion exchange method in achieving a uniform Cu distribution. The ion-exchange conditions, product compositions and Cu contents are listed in Table 1. After the direct ion exchange process, the compositions of all the samples have invisible changes. The Cu content can be adjusted from 1.75 wt% to 4.64 wt% by altering the concentrations of the  $\text{Cu}(\text{Ac})_2$  solution. Meanwhile, it should be noted that the Cu-exchange capacity are affected by the Si content of SAPO-56 precursors. Comparing the ion-exchange conditions of S56-0.13Si-3.7Cu, S56-0.16Si-3.6Cu and

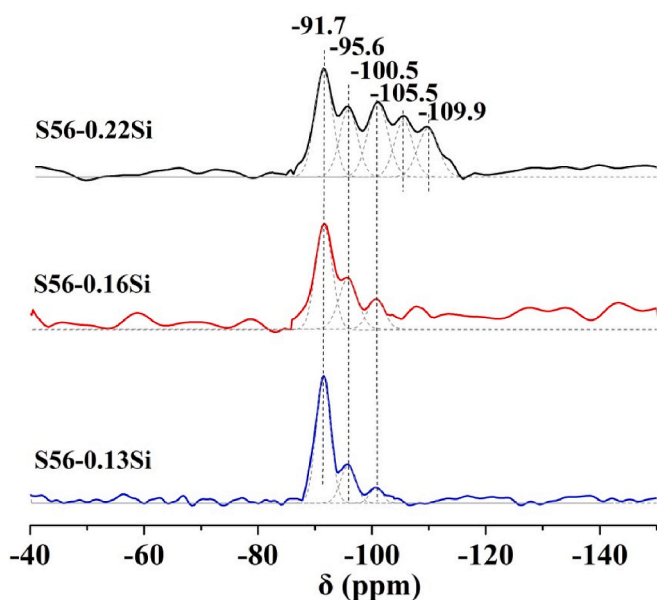


Fig. 3.  $^{29}\text{Si}$  MAS NMR spectra of S56-0.13Si, S56-0.16Si and S56-0.22Si.

Table 3

The content of different Si environments based on  $^{29}\text{Si}$  NMR results.

Sample	Si(4Al)	Si(3Al)	Si(2Al)	Si(1Al)	Si-islands
S56-0.13Si	0.093	0.021	0.016	0	0
S56-0.16Si	0.083	0.039	0.040	0	0
S56-0.22Si	0.066	0.033	0.064	0.030	0.031

S56-0.22Si-3.8Cu, SAPO-56 with higher Si content needs a lower Cu (Ac)<sub>2</sub> concentration to achieve the similar Cu loading. This result indicates SAPO-56 with higher Si content has a stronger Cu-exchange ability. The SEM image of S56-0.13Si-3.7Cu (Fig. 2) reveals that the sample remains hexagonal platelet morphology with similar particle sizes after ion-exchange process.

N<sub>2</sub> adsorption measurements were conducted to test the textural properties, and the results are listed in Table 2. The micropore surface area and micropore volumes of S56-0.13 are 534 m<sup>2</sup> g<sup>-1</sup> and 0.26 cm<sup>3</sup> g<sup>-1</sup>, respectively, confirming a good crystallinity of the as-synthesized SAPO-56. After the direct ion exchange behavior, the micropore surface area and micropore volumes of the Cu-SAPO-34 samples have a slight decrease. As the Cu-SAPO-56 with higher Cu content has a bigger decline, the reduced micropore surface area and micropore volumes are probably caused by the occupation of framework channels by the exchanged Cu species.

It is well accepted that the chemical environments of the Si are crucial for both acid sites and Cu-exchange process. The Si environments of SAPO-56 and Cu-SAPO-56 were investigated using solid-state  $^{29}\text{Si}$  MAS NMR, and the spectra are shown in Fig. 3 and Fig. S1. In the spectrum of S56-0.13Si (in Fig. 3), a strong signal at -91.7 ppm and two weak signals at -95.6 ppm and -100.5 ppm are observed which attributed to the Si(4Al) environments, Si(3Al) environments and Si(2Al) environments, respectively [26]. The spectrum of S56-0.16Si also shows these three signals. However, the peak strength of Si(3Al) environments and Si(2Al) environments becomes stronger. For the spectrum of S56-0.22Si with the highest Si content, the above two peaks are further increased while two new peaks at -105.5 ppm and 109.9 ppm are observed which correspond to the Si(1Al) environments and Si-islands, respectively [26]. To estimate the amounts of different Si environments in the as-synthesized SAPO-56 samples, the  $^{29}\text{Si}$  MAS NMR spectra are deconvoluted by Lorentzian method. The quantification results are listed in Table 3. Even though S56-0.22Si has the highest

Si content, the Si(4Al) environment of S56-0.22Si is less than those of S56-0.16Si and S56-0.22S. It is due to the Si aggregation. Thus, most of the increased Si atoms formed Si(nAl) (n = 1–3) environment while the amount of Si islands in S56-0.22Si only accounts for a small proportion (about 15 %) of the whole Si content. As shown in Fig. S1, the  $^{29}\text{Si}$  MAS NMR spectra of S56-0.13Si-3.7Cu, S56-0.16Si-3.6Cu and S56-0.22Si-3.8Cu are similar to the spectra of their precursors (S56-0.13Si, S56-0.16Si and S56-0.22Si). Therefore, the Si environments of Cu-SAPO-56 are basically maintained after direct ion exchange process.

It is well known that there are two Si insertion mechanisms in the crystallization of SAPO framework. The first one denoted SM2 is the substitution of P atom by Si atom, which results in the formation of Si(4Al) environments. The other one denoted as SM3 is double replacement of adjacent P atom and Al atom by two Si atoms, which generates Si(nAl) (n = 3–0) environments [27,28]. As the SM3 produces more protons, the Brønsted acid sites formed by this Si insertion mechanism are stronger. The  $^{29}\text{Si}$  MAS NMR results indicate the insertion of Si atoms in SAPO-56 firstly follow SM2 indicating the generation of abundant Si(4Al) environments. However, as the P substitution sites are limited, the exceeded Si atoms have to follow SM3 and form Si(nAl) (n = 3–0) environments with stronger Brønsted acidity.

### 3.2. NH<sub>3</sub>-SCR performance of the Cu-SAPO-56 catalysts

The catalytic performances of Cu-SAPO-56 samples were evaluated under standard NH<sub>3</sub>-SCR conditions at a GHSV of 180,000 h<sup>-1</sup>. The reaction results are presented in Fig. 4(a) and (b). All the samples exhibit good NH<sub>3</sub>-SCR activities. The samples give the NO<sub>x</sub> conversion of 16–43 % and 28–85 % at 150 °C and 175 °C, respectively. When the reaction temperature rises to 200 °C, the NO<sub>x</sub> conversion quickly increases to more than 90 %. This high NO<sub>x</sub> conversion maintains until 400 °C. Then, the NO<sub>x</sub> conversion drops to 67–87 % at 500 °C, which is probably caused by the undesired NH<sub>3</sub> oxidation reaction [29,30]. Comparing the catalytic performances of Cu-SAPO-56 with different Cu content (as shown in Fig. 4(a)), Cu-SAPO-56 with more Cu content has a higher NO<sub>x</sub> conversion at low temperature range but a lower NO<sub>x</sub> conversion at high temperature range. And the influence of Si content in Cu-SAPO-56 to the NH<sub>3</sub>-SCR activity is complicated (as shown in Fig. 4(b)). Among the three Cu-SAPO-56 samples with different Si content, S56-0.13Si-3.7Cu has the highest low temperature NO<sub>x</sub> conversion. Meanwhile, the low temperature NO<sub>x</sub> conversion of S56-0.22Si-3.8Cu is higher than that of S56-0.16Si-3.6Cu.

To investigate the high temperature hydrothermal stability of Cu-SAPO-56, all the samples were steam treated at 800 °C for 16 h. Then, the catalytic performances of the steam treated Cu-SAPO-56 were evaluated. As shown in Fig. 4(c) and (d), most of the Cu-SAPO-56 samples maintain more than 90 % NO<sub>x</sub> conversion at 250–400 °C. The results prove the Cu-SAPO-56 has a good high temperature hydrothermal stability. According to the NO<sub>x</sub> conversion of steam treated S56-0.22Si-3.8Cu and S56-0.132Si-4.6Cu, the excess Cu content and Si content have negative effects on the high temperature hydrothermal stability of Cu-SAPO-56. As shown in Fig. S2, all the Cu-SAPO-56 samples exhibit high N<sub>2</sub> selectivity before and after high temperature steam treatment. The fresh samples give almost 100 % N<sub>2</sub> selectivity at 150–400 °C. When the reaction temperature rises to 500 °C, the N<sub>2</sub> selectivity is decreased because of the competition of NH<sub>3</sub> oxidation.

Cu-SAPO-56 samples were also steam treated at 50 °C for 24 h to test the low temperature hydrothermal stability. As shown in Fig. S3, all the samples exhibit excellent low temperature hydrothermal stability. The NO<sub>x</sub> conversion maintains more than 85 % at 200–450 °C. It is surprised to find the low temperature hydrothermal treatment is helpful to improve the high temperature NO<sub>x</sub> conversion of Cu-SAPO-56. Moreover, the higher Si content and lower Cu content are benefit to the low temperature hydrothermal stability of Cu-SAPO-56.

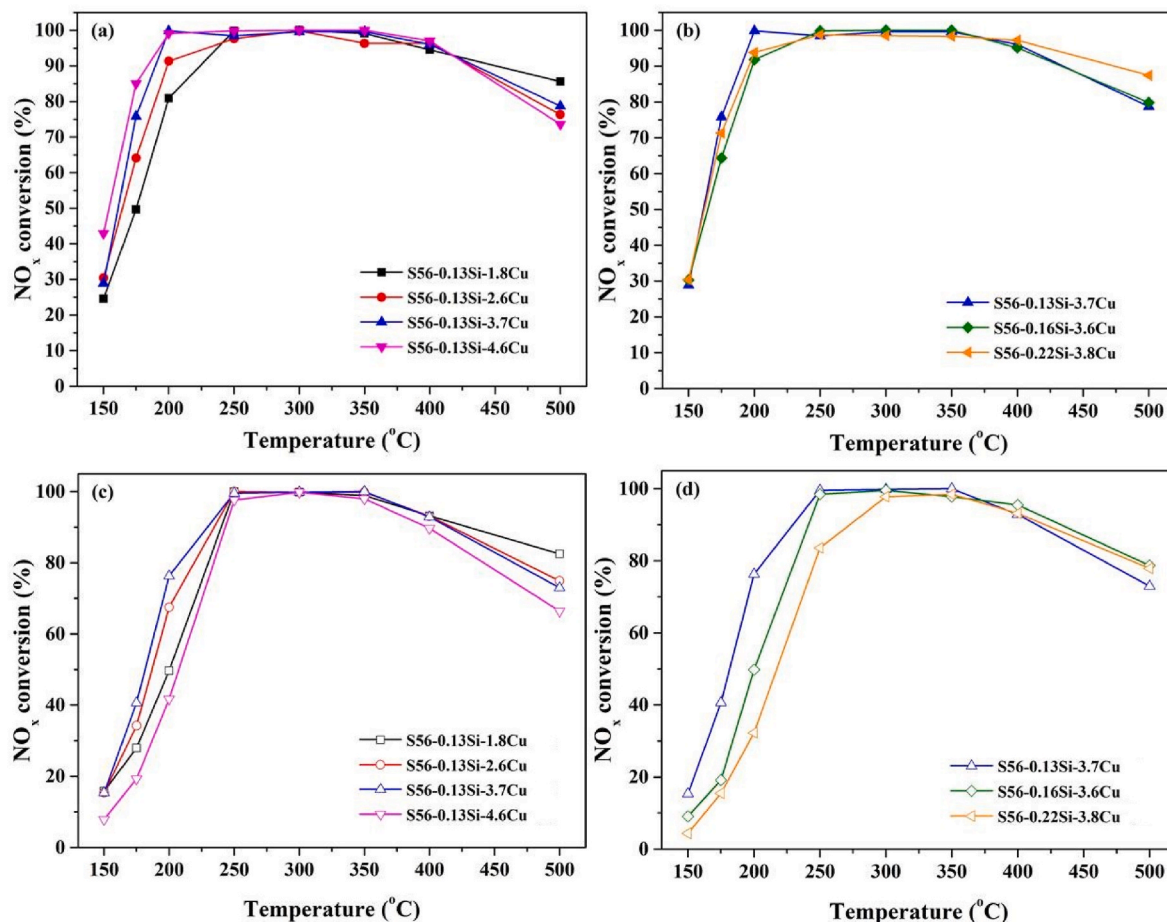


Fig. 4. NO<sub>x</sub> conversion as a function of reaction temperature over (a) fresh and (c) high-temperature steam treated S56-0.13Si-1.8Cu, S56-0.13Si-2.6Cu, S56-0.13Si-3.7Cu and S56-0.13Si-4.6Cu; (b) fresh and (d) high-temperature steam treated S56-0.13Si-3.7Cu, S56-0.16Si-3.6Cu and S56-0.22Si-3.8Cu. The feed contains 500 ppm of NO, 500 ppm of NH<sub>3</sub>, 6.1 % of O<sub>2</sub>, 6.4 % of H<sub>2</sub>O and balanced with N<sub>2</sub> at 180,000 h<sup>-1</sup> gas hourly space velocity.

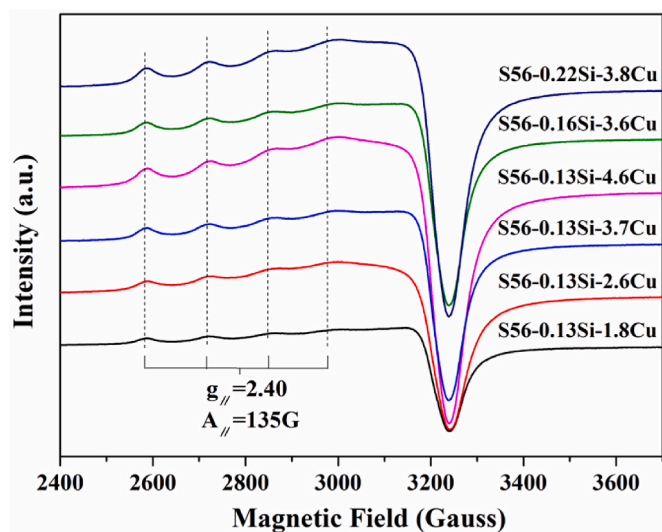


Fig. 5. EPR spectra of the samples.

### 3.3. Cu species characterization

According to the catalytic reaction results, Cu species play crucial roles in the NH<sub>3</sub>-SCR performance. EPR analysis was employed to analyze the isolated Cu<sup>2+</sup> ions in Cu-SAPO-56. As shown in Fig. 5, all the

Table 4

Isolated Cu<sup>2+</sup> ions contents of the samples from EPR results.

Sample	Cu <sup>2+</sup> content ( wt% )	Cu <sup>2+</sup> /Cu (%)
S56-0.13Si-1.8Cu	0.80	45.7
S56-0.13Si-2.6Cu	1.31	49.6
S56-0.13Si-3.7Cu	1.70	46.3
S56-0.13Si-4.6Cu	2.11	45.5
S56-0.16Si-3.6Cu	1.83	50.3
S56-0.22Si-3.8Cu	2.09	55.6

samples have only one signal at  $g_{\parallel} = 2.40$  and  $A_{\parallel} = 135$  G, which is assigned to the isolated Cu<sup>2+</sup> ions located at the double 6-ring [31]. The amounts of isolated Cu<sup>2+</sup> ion have been estimated from the EPR spectra, and the results are listed in Table 4. The Cu<sup>2+</sup> ion contents are lower than the Cu loading tested by XRF which indicates the existence of other Cu species. This phenomenon is probably caused by the limited Cu-exchange sites (located in hydroxyl sites of Si-OH-Al). Thus, the exceeded exchanged Cu ions have to form other Cu species. Although Cu-SAPO-56 with higher Cu content possesses more isolated Cu<sup>2+</sup> ions. The ratio of isolated Cu<sup>2+</sup> ions in this kind of Cu-SAPO-56 is decreased. Meanwhile, it should be noted that the higher Si content in Cu-SAPO-56 is helpful to raise the proportion of Cu<sup>2+</sup> ions, which is attributed to the formation of more Si-OH-Al environments.

As different Cu species can be distinguished by their reduction temperatures, H<sub>2</sub>-TPR was carried out to probe the Cu species in Cu-SAPO-56. As shown in Fig. 6, the TPR profiles of the samples present four main reduction peaks at ca. 150–210 °C, 210–320 °C, 320–550 °C

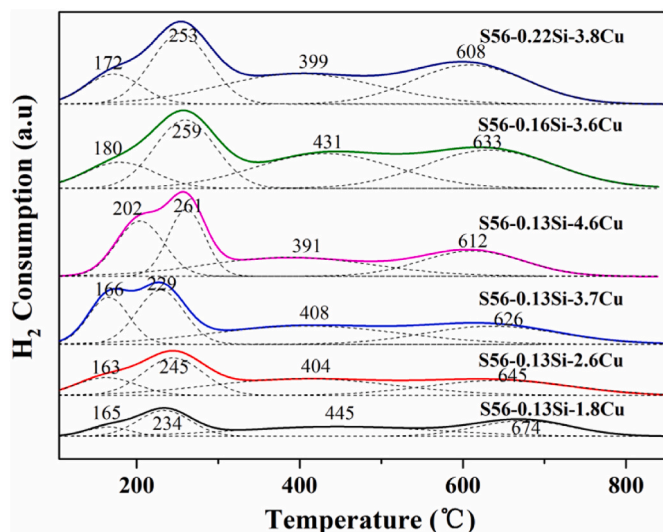


Fig. 6. H<sub>2</sub>-TPR profiles of the samples.

Table 5  
Different Cu species contents based on H<sub>2</sub>-TPR results.

Sample	Surface CuO (wt %)	Cu <sup>2+</sup> (wt %)	CuO (wt %)	Cu <sup>+</sup> (wt %)
S56-0.13Si-1.7Cu	0.13	0.90	0.64	0.08
S56-0.13Si-2.6Cu	0.33	1.36	0.94	0.01
S56-0.13Si-3.7Cu	0.67	1.79	1.20	0.01
S56-0.13Si-4.6Cu	1.10	2.07	1.34	0.13
S56-0.16Si-3.6Cu	0.40	1.83	1.27	0.14
S56-0.22Si-3.8Cu	0.40	2.02	1.18	0.16

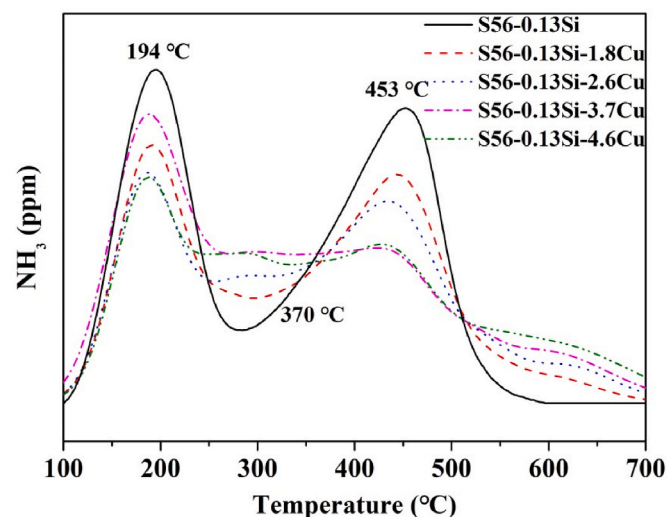


Fig. 7. NH<sub>3</sub>-TPD profiles of S56-0.13Si, S56-0.13Si-1.8Cu, S56-0.13Si-2.6Cu, S56-0.13Si-3.7Cu and S56-0.13Si-4.6Cu.

and 550–800 °C. The four reduction peaks are attributed to the reduction of surface CuO to Cu<sup>0</sup>, the reduction of isolated Cu<sup>2+</sup> to Cu<sup>+</sup>, the reduction of bulk CuO to Cu<sup>0</sup> and the reduction of Cu<sup>+</sup> to Cu<sup>0</sup> [32–34]. By regression analysis of H<sub>2</sub>-TPR profiles, the quantities of different Cu

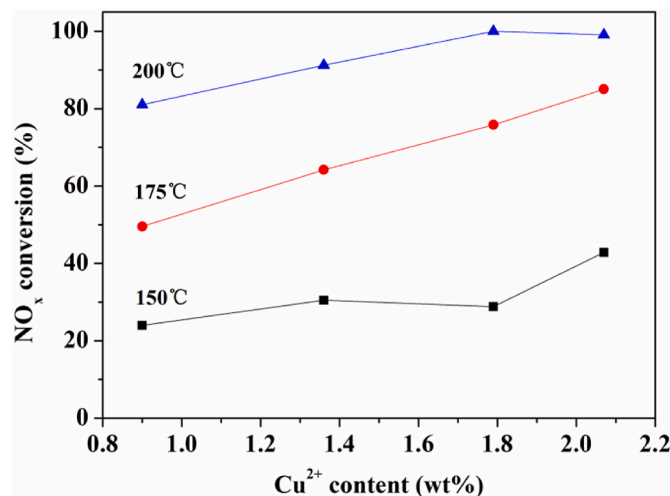


Fig. 8. The change of NO<sub>x</sub> conversion with Cu<sup>2+</sup> ion content of Cu-SAPO-56 under different temperatures.

species are listed in Table 5. The amount of Cu<sup>2+</sup> ions is similar to the estimated results of EPR. According to the regression analysis, the Cu species in Cu-SAPO-56 are mainly Cu<sup>2+</sup> ions and CuO as well as a bit of Cu<sup>+</sup> ions. With the increasing of the Cu content, the proportion of CuO grows from 44 % to 53 %.

### 3.4. Investigation of the catalyst acidity

The NH<sub>3</sub>-TPD was employed to determine the density and strength of different acid sites. The NH<sub>3</sub>-TPD profiles of the SAPO-56 are displayed in Fig. S4. Each desorption curves can be decomposed into three peaks centered at ca. 194 °C (assigned to weak acid sites from surface hydroxyl groups), 370 °C (assigned to moderate Brønsted acid sites), and 453 °C (assigned to strong Brønsted acid sites) [35,36]. Moreover, the area of desorption peak in NH<sub>3</sub>-TPD profiles are listed in Table S1 by regression analysis. Compared to S56-0.31Si, there are more strong Brønsted acid sites but less moderate Brønsted acid sites in S56-0.16Si and S56-0.22Si. This result is consistent with the Si environments analyzed by <sup>29</sup>Si MAS NMR.

As shown in Fig. 7, the NH<sub>3</sub>-TPD profiles of (S56-0.13Si-1.8Cu, S56-0.13Si-2.6Cu, S56-0.13Si-3.7Cu and S56-0.13Si-4.6Cu) exhibit the influence of the Cu content to the acidity of S56-0.13Si and its ion-exchange derivatives Cu-SAPO-56. Cu-SAPO-56 with higher Cu content contains a larger area of moderate acid desorption peak and a higher desorption temperature. Meanwhile, its strong acid desorption peak shows a contrary tendency. Thus, after Cu ion exchange, the strong Brønsted acid sites are replaced by the exchanged Cu ions and transform to Lewis acid sites during the ion-exchange process. And the new Lewis acid site has a stronger acidity than the original moderate Brønsted acid site.

### 3.5. The relationship between NH<sub>3</sub>-SCR performance and Cu/Si species

Based on the above experimental results and analyses, we next discuss the influences of Cu species and acidity to the NH<sub>3</sub>-SCR activity. As shown in Fig. 8, the NO<sub>x</sub> conversion is almost in proportionate to the Cu<sup>2+</sup> ion content of Cu-SAPO-56 at low temperature range. As the NH<sub>3</sub>-SCR activity at low temperature range is influenced by the amount of active sites in catalysts [37], the isolate Cu<sup>2+</sup> ions located in D6R cages are the active sites of NH<sub>3</sub>-SCR reaction. However, the excess Cu content in Cu-SAPO-56 is harm to the NH<sub>3</sub>-SCR performance at high temperature range. It should be attributed to the high proportion of CuO which promotes the undesired NH<sub>3</sub> oxidation reaction. Meanwhile, the undesirable hydrothermal stability of S56-0.13Si-4.6Cu is probably due to

the existence of abundant CuO.

S56–0.13Si-2.6Cu with lower Cu<sup>2+</sup> ion content exhibits similar NH<sub>3</sub>-SCR activity at low temperature range compared to S56–0.16Si-3.6Cu. The gap of NH<sub>3</sub>-SCR activity for S56–0.13Si-2.6Cu caused by the lower Cu<sup>2+</sup> ion content is probably filled by its weaker acidity, which promotes the NH<sub>3</sub> diffusion to Cu<sup>2+</sup> ion activity sites and accelerates the reaction rate [36]. Thus, S56–0.22Si-3.8Cu exhibiting a better low temperature NH<sub>3</sub>-SCR activity than S56–0.16Si-3.6Cu is probably caused by its higher Cu<sup>2+</sup> ions content. And the bad hydrothermal stability of S56–0.22Si-3.8Cu is due to the existence of Si-islands, which are more easily to be attacked by H<sub>2</sub>O during the steam treatment.

#### 4. Conclusion

In conclusion, Cu-SAPO-56 prepared by direct ion exchange method gives a NH<sub>3</sub>-SCR catalyst that exhibits excellent activity over a wide temperature window even after severe hydrothermal aging (800 °C for 16 h or 50 °C for 24 h). All the isolated Cu<sup>2+</sup> ions are located in D6R cages and proved to be the active sites of NH<sub>3</sub>-SCR reaction. Both Cu content and Si content in Cu-SAPO-56 play significant roles in NH<sub>3</sub>-SCR reactions. The higher Cu content makes Cu-SAPO-56 have more Cu<sup>2+</sup> ions and CuO. Thus, raising Cu content is benefit to the low temperature NH<sub>3</sub>-SCR activity but harm to the high temperature NH<sub>3</sub>-SCR activity and hydrothermal stability. The influence of Si environment in Cu-SAPO-56 to the low temperature NH<sub>3</sub>-SCR performance is complicated. Even though the higher Si content in Cu-SAPO-56 is helpful to raise the proportion of Cu<sup>2+</sup> ions, weaker acidity in Cu-SAPO-56 is also benefit to the low temperature NH<sub>3</sub>-SCR activity. Meanwhile, the excess Si content is bad for high temperature hydrothermal stability which is due to the formation of Si-islands.

#### CRediT authorship contribution statement

**Lei Xu:** Formal analysis. **Ye Wang:** Formal analysis. **Yi Cao:** Investigation. **Feng Zhang:** Investigation. **Yu Song:** Investigation. **Chunling Yu:** Investigation. **Peng Tian:** Conceptualization. **Lijing Sun:** Writing – review & editing, Writing – original draft, Investigation, Formal analysis.

#### Declaration of competing interest

The authors declare that they have no known competing financial interests or personal relationships that could have appeared to influence the work reported in this paper.

#### Data availability

Data will be made available on request.

#### Acknowledgements

This work was supported by the National Natural Science Foundation of China (Grant No. 21991091).

#### Appendix A. Supplementary data

Supplementary data to this article can be found online at <https://doi.org/10.1016/j.micromeso.2023.112978>.

#### References

- [1] Y.K. Park, B.S. Kim, Catalytic removal of nitrogen oxides (NO, NO<sub>2</sub>, N<sub>2</sub>O) from ammonia-fueled combustion exhaust: a review of applicable technologies, *Chem. Eng. J.* 461 (2023) 141958.
- [2] Q. Sun, N. Wang, J. Yu, Advances in catalytic applications of zeolite-supported metal catalysts, *Adv. Mater.* 33 (2021) 2104442.
- [3] F. Gramigni, U. Iacobone, N.D. Nasello, T. Selli, N. Usberti, I. Nova, Review of hydrocarbon poisoning and deactivation effects on Cu-Zeolite, Fe-Zeolite, and vanadium-based selective catalytic reduction catalysts for NOx removal from lean exhausts, *Ind. Eng. Chem. Res.* 60 (2021) 6403–6420.
- [4] M. Iwamoto, H. Furukawa, Y. Mine, F. Uemura, S. Mikuriya, S. Kagawa, Copper(II) ion-exchanged ZSM-5 zeolites as highly active catalysts for direct and continuous decomposition of nitrogen monoxide, *J. Chem. Soc. Chem. Commun.* (1986) 1272–1273.
- [5] H. Wang, R. Xu, Y. Jin, R. Zhang, Zeolite structure effects on Cu active center, SCR performance and stability of Cu-zeolite catalysts, *Catal. Today* 327 (2019) 295–307.
- [6] P.G. Blakeman, E.M. Burkholder, H. Chen, J.E. Collier, J.M. Fedeyko, H. Jobson, R. Rajaram, The role of pore size on the thermal stability of zeolite supported Cu SCR catalysts, *Catal. Today* 231 (2014) 56–63.
- [7] S. Mohan, P. Dinesha, S. Kumar, NOx reduction behaviour in copper zeolite catalysts for ammonia SCR systems: a review, *Chem. Eng. J.* 384 (2020) 123253.
- [8] S.T. Korhonen, D.W. Fickel, R.F. Lobo, B.M. Weckhuysen, A.M. Beale, Isolated Cu<sup>2+</sup> ions: active sites for selective catalytic reduction of NO, *Chem. Commun.* 47 (2011) 800–802.
- [9] J. Chen, B. Guan, Z. Liu, X. Wu, J. Guo, C. Zheng, J. Zhou, T. Su, P. Han, C. Yang, Y. Zhang, B. Qin, J. Gao, Y. Yuan, W. Xie, N. Zhou, Z. Huang, Review on advances in structure–activity relationship, reaction & deactivation mechanism and rational improving design of selective catalytic reduction deNO<sub>x</sub> catalysts: challenges and opportunities, *Fuel* 343 (2023) 127924.
- [10] W. Shan, H. Song, Catalysts for the selective catalytic reduction of NO<sub>x</sub> with NH<sub>3</sub> at low temperature, *Catal. Sci. Technol.* 5 (2015) 4280–4288.
- [11] S. Han, W. Rao, J. Hu, X. Tang, Y. Ma, J. Du, Z. Liu, Q. Wu, Y. Ma, X. Meng, W. Shan, F. Xiao, H. He, Direct synthesis of high silica SSZ-16 zeolite with extraordinarily superior performance in NH<sub>3</sub>-SCR reaction, *Appl. Catal. B Environ.* 332 (2023) 122746.
- [12] D. Jo, G.T. Park, Ta Ryu, S.B. Hong, Economical synthesis of high-silica LTA zeolites: a step forward in developing a new commercial NH<sub>3</sub>-SCR catalyst, *Appl. Catal. B Environ.* 243 (2019) 212–219.
- [13] D.W. Fickel, E. D'Addio, J.A. Lauterbach, R.F. Lobo, The ammonia selective catalytic reduction activity of copper-exchanged small-pore zeolites, *Appl. Catal. B Environ.* 102 (2011) 441–448.
- [14] Y.J. Kim, P.S. Kim, C.H. Kim, Deactivation mechanism of Cu/Zeolite SCR catalyst under high-temperature rich operation condition, *Appl. Catal. A-Gen.* 569 (2019) 175–180.
- [15] H. Zhao, X. Wu, Z. Huang, Z. Chen, G. Jing, A comparative study of the thermal and hydrothermal aging effect on Cu-SSZ-13 for the selective catalytic reduction of NO<sub>x</sub> with NH<sub>3</sub>, *Chin. J. Chem. Eng.* 45 (2022) 68–77.
- [16] J. Wang, H. Zhao, G. Haller, Y. Li, Recent advances in the selective catalytic reduction of NOx with NH<sub>3</sub> on Cu-Chabazite catalysts, *Appl. Catal. B Environ.* 202 (2017) 346–354.
- [17] D. Wang, Y. Jangjou, Y. Liu, M.K. Sharma, J. Luo, J. Li, K. Kamasamudram, W. S. Epling, A comparison of hydrothermal aging effects on NH<sub>3</sub>-SCR of NOx over Cu-SSZ-13 and Cu-SAPO-34 catalysts, *Appl. Catal. B Environ.* 165 (2015) 438–445.
- [18] Y. Shan, W. Shan, X. Shi, J. Du, Y. Yu, H. He, A comparative study of the activity and hydrothermal stability of Al-rich Cu-SSZ-39 and Cu-SSZ-13, *Appl. Catal. B Environ.* 264 (2020) 118511.
- [19] R. Martínez-Franco, M. Moliner, A. Corma, Direct synthesis design of Cu-SAPO-18, a very efficient catalyst for the SCR of NOx, *J. Catal.* 319 (2014) 36–43.
- [20] W. Su, Z. Li, Y. Peng, J. Li, Correlation of the changes in the framework and active Cu sites for typical Cu/CHA zeolites (SSZ-13 and SAPO-34) during hydrothermal aging, *Phys. Chem. Chem. Phys.* 17 (2015) 29142–29149.
- [21] L. Wang, J.R. Gaudet, W. Li, D. Weng, Migration of Cu species in Cu/SAPO-34 during hydrothermal aging, *J. Catal.* 306 (2013) 68–77.
- [22] F. Gao, E.D. Walter, N.M. Washton, J. Szanyi, C.H.F. Peden, Synthesis and evaluation of Cu-SAPO-34 catalysts for ammonia selective catalytic reduction. 1. Aqueous solution ion exchange, *ACS Catal.* 3 (2013) 2083–2093.
- [23] X. Xiang, M. Yang, B. Gao, Y. Qiao, P. Tian, S. Xu, Z. Liu, Direct Cu<sup>2+</sup> ion-exchanged into as-synthesized SAPO-34 and its catalytic application in the selective catalytic reduction of NO with NH<sub>3</sub>, *RSC Adv.* 6 (2016) 12544–12552.
- [24] T. Wu, X. Feng, M.L. Carreon, M.A. Carreon, Synthesis of SAPO-56 with controlled crystal size, *J. Nanoparticle Res.* 93 (2017), <https://doi.org/10.1007/s11051-017-3772-3>.
- [25] X. Xiang, M. Yang, B. Gao, Y. Qiao, P. Tian, S. Xu, Z. Liu, Direct Cu<sup>2+</sup> ion-exchanged into as-synthesized SAPO-34 and its catalytic application in the selective catalytic reduction of NO with NH<sub>3</sub>, *RSC Adv.* 6 (2016) 12544.
- [26] W. Shen, X. Li, Y. Wei, P. Tian, F. Deng, X. Han, X. Bao, A study of the acidity of SAPO-34 by solid-state NMR spectroscopy, *Microporous Mesoporous Mater.* 158 (2012) 19–25.
- [27] A. Buchholz, W. Wang, M. Xu, A. Arnold, M. Hunger, Thermal stability and dehydroxylation of Bronsted acid sites in silicoaluminophosphates H-SAPO-11, H-SAPO-81 H-SAPO-31, and H-SAPO-34 investigated by multi-nuclear solid-state NMR spectroscopy, *Microporous Mesoporous Mater.* 56 (2002) 267–278.
- [28] J. Tan, Z. Liu, X. Bao, X. Liu, X. Han, C. He, R. Zhai, Crystallization and Si incorporation mechanisms of SAPO-34, *Microporous Mesoporous Mater.* 53 (2002) 97–108.
- [29] Y. Zheng, Y. Guo, J. Wang, L. Luo, T. Zhu, Ca doping effect on the competition of NH<sub>3</sub>-SCR and NH<sub>3</sub> oxidation reactions over vanadium-based catalysts, *J. Phys. Chem. C* 125 (2021) 6128–6136.
- [30] Y. Jangjou, M. Ali, Q. Chang, D. Wang, J. Li, A. Kumar, W.S. Epling, Effect of SO<sub>2</sub> on NH<sub>3</sub> oxidation over a Cu-SAPO-34 SCR catalyst, *Catal. Sci. Technol.* 6 (2016) 2679–2685.

- [31] Y. Cao, D. Fan, P. Tian, L. Cao, T. Sun, S. Xu, M. Yang, Z. Liu, The influence of low-temperature hydration methods on the stability of Cu-SAPO-34 SCR catalyst, *Chem. Eng. J.* 354 (2018) 85–92.
- [32] L. Sun, M. Yang, L. Cao, Y. Cao, S. Xu, D. Zhu, P. Tian, Z. Liu, Fabrication of Cu-CHA composites with enhanced NH<sub>3</sub>-SCR catalytic performances and hydrothermal stabilities, *Microporous Mesoporous Mater.* 309 (2020) 110585.
- [33] C. Niu, X. Shi, F. Liu, K. Liu, L. Xie, Y. You, H. He, High hydrothermal stability of Cu-SAPO-34 catalysts for the NH<sub>3</sub>-SCR of NO<sub>x</sub>, *Chem. Eng. J.* 294 (2016) 254–263.
- [34] J. Wang, T. Yu, X. Wang, G. Qi, J. Xue, M. Shen, W. Li, The influence of silicon on the catalytic properties of Cu/SAPO-34 for NO<sub>x</sub> reduction by ammonia-SCR, *Applied Appl. Catal. B-Environ.* 127 (2012) 137–147.
- [35] Y. Cao, D. Fan, P. Tian, L. Cao, T. Sun, S. Xu, M. Yang, Z. Liu, The influence of low-temperature hydration methods on the stability of Cu-SAPO-34 SCR catalyst, *Chem. Eng. J.* 354 (2018) 85–92.
- [36] L. Sun, M. Yang, Y. Cao, P. Tian, P. Wu, L. Cao, S. Xu, S. Zeng, Z. Liu, A reconstruction strategy for the synthesis of Cu-SAPO-34 with excellent NH<sub>3</sub>-SCR catalytic performance and hydrothermal stability, *Chin. J. Catal.* 41 (2020) 1410–1420.
- [37] J. Xue, X. Wang, G. Qi, J. Wang, M. Shen, W. Li, Characterization of copper species over Cu/SAPO-34 in selective catalytic reduction of NO<sub>x</sub> with ammonia: relationships between active Cu sites and de-NO<sub>x</sub> performance at low temperature, *J. Catal.* 297 (2013) 56–64.